# Transition Metal Azahemiporphycenes as Singlet Oxygen Sensitizers

Abraham B. Alemayehu,[a] Kevin J. Gagnon,[a] Yoann Rousselin,[c] Max Schmallegger,[d] Sergey M. Borisov*,[e] and Abhik Ghosh*,[a]

[a]Department of Chemistry, University of Tromsø, N-9037 Tromsø, Norway

[b]Advanced Light Source, Lawrence Berkeley National Laboratory, Berkeley, CA 94720-8229, USA

[c]ICMUB, UMR CNRS 6302, Université Bourgogne Franche-Comte, BP 47870, 21078 Dijon Cedex, France

[d]Institute of Analytical Chemistry and Food Chemistry, Graz University of Technology, Stremayrgasse 9, 8010 Graz, Austria

[e]Institute of Physical and Theoretical Chemistry, Graz University of Technology, Stremayrgasse 9, 8010 Graz, Austria

Email: sergey.borisov@tugraz.at (SMB); abhik.ghosh@uit.no (AG)

**Abstract.** Using free-base tris(*p*-X-phenyl)corrole (X = H, Me, OMe) as starting materials and 4-aminotriazole as the nitrogen source, we used a DDQ-mediated, room-temperature strategy for generating isocorrole synthesis to obtain the corresponding 6-azahemiporphycenes, $H_2$[X-AHP], one of which was structurally characterized with single-crystal X-ray diffraction analysis. The free-base ligands were readily derivatized to their Pd(II), Pt(II), and Mn(II) complexes; of these, one Pd(II) complex was structurally characterized. Three of the complexes, M[Me-AHP] (M = Pd, Pt, Mn), were singled out for photophysical and singlet oxygen sensitization studies. Although none of the new complexes proved luminescent, Pd[Me-AHP] was found to be an excellent singlet oxygen sensitizer, with a singlet oxygen quantum yield of 84% in 9:1 v/v ethanol:tetrahydrofuran at room temperature. The corresponding value for Pt[Me-AHP] was found to be only 11% and that for Mn[Me-AHP] essentially 0%. These singlet oxygen quantum yields were consonant with triplet lifetimes accessed via transition absorption spectroscopy. Combined with their strong absorption in the red, these findings suggest that palladium 6-azahemiporphycenes are worthy of exploration as a new class of triplet photosensitizers for photodynamic therapy of cancer and other diseases.

## INTRODUCTION

As aromatic compounds, porphyrins and related macrocycles undergo a wide range of electrophilic substitution reactions, leading to a correspondingly wide range of functionalized derivatives.[1,2] Less widely appreciated are reactions effecting skeletal rearrangements and alterations to the $N_4$ core of the molecules.[3,4] Several of these reactions afford exotic macrocycles that cannot be readily accessed by other means. An excellent example of such a reaction is the ring expansion of a corrole to a 6-azahemiporphycene ($H_2$[AHP]) via interaction with a nitrogen atom source.[5,6,7,8] A related example involves the ring expansion of a corrole to a hemiporphycene.[9,10] Several transition metal derivatives of (aza)hemiporphycenes have been reported, but by and large their electrochemical, optical and photophysical properties remain inadequately explored. The intriguing question as to their suitability as photosensitizers in photodynamic therapy also remains unanswered. Herein we have made an attempt to shed light in these questions, focusing on manganese, palladium and platinum complexes of 6-azahemiporphycenes (Chart 1).

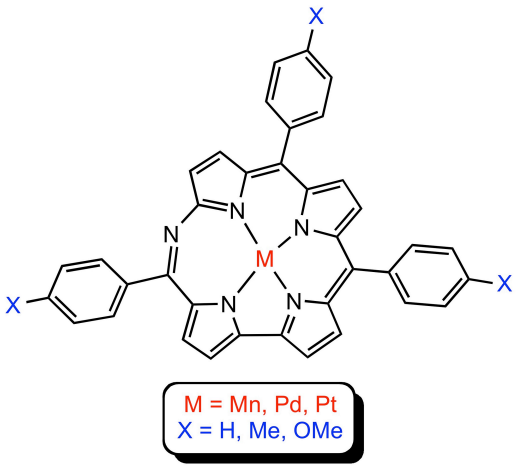


Chart 1. Complexes studied in this work.

## RESULTS AND DISCUSSION

**(a) Synthesis of free-base and transition metal derivatives.** As a prelude to systematic studies of transition metal derivatives, we chose to optimize the literature synthesis of free-base 6-azahemiporphycenes. The reported method consists of the interaction of a free-base *meso*-triarylcorrole with 4-aminotriazole in the presence of potassium hydroxide in refluxing toluene.[6] In our hands, the protocol led to somewhat inconsistent yields. The reported involvement of isocorrole intermediates suggested an improved synthetic strategy. Following a recent synthesis

of pyrrole-appended isocorroles in one of our laboratories,[11] we attempted to generate the key isocorrole intermediate by oxidizing a free-base corrole with DDQ in dichloromethane at room temperature and trapping the resulting cation-radical with 4-aminotriazole. The new method indeed led to the desired 6-azahemiporphycene but in rather poor yields. Dissolving the 4-aminotriazole in methanol, which we surmised might help, also proved unsatisfactory in that methanol was found to compete with 4-aminotriazole as a nucleophile, thus degrading the yield of the azahemiporphycene. Warming also did not confer any advantages, resulting simply in increased reversion of the corrole cation-radical to the neutral free base. It appeared that a polar solvent was needed, which would dissolve 4-aminotriazole but would not attack the corrole cation radical. Dimethyl sulfoxide (DMSO) fit the bill. The final, optimized conditions consisted of dissolving a free-base corrole and one equivalent of DDQ in dichloromethane, adding 5 equivalents of 4-aminotriazole dissolved in DMSO and KOH, and stirring overnight at room temperature. At that point, UV-vis and HRMS analysis of the reaction mixture indicated complete disappearance of the free-base corrole, with the 6-azahemiporphycene as the sole porphyrinoid product. Standard work-up resulted in the isolation of the free-base AHP in 49 to 58 % yield (Scheme 1).

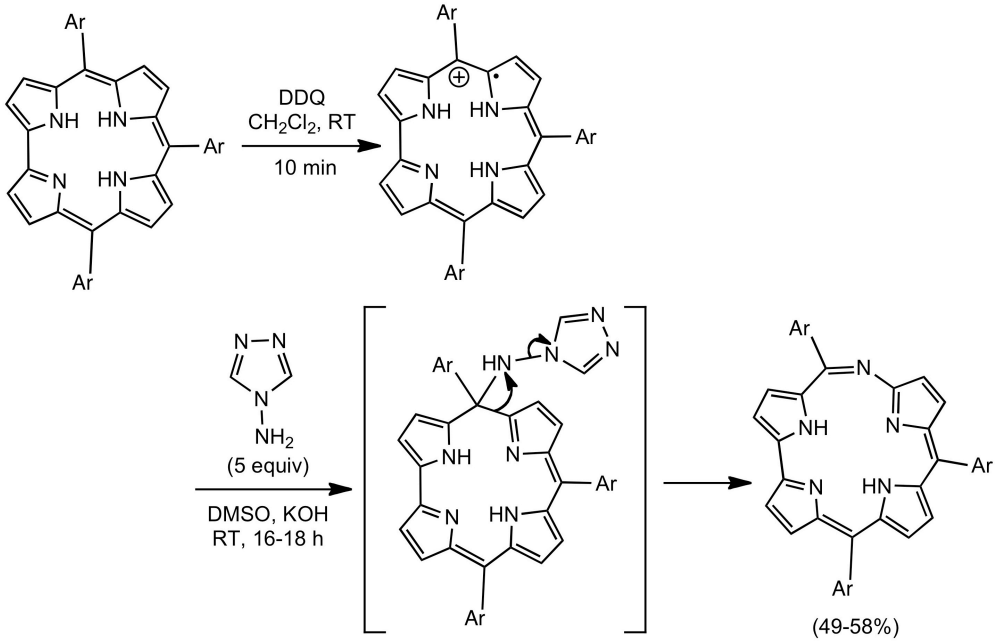


Scheme 1. Optimized room-temperature synthesis of 6-azahemiporphycenes.

Transition metal AHP derivatives, M[X-AHP], were synthesized with three different *para* substituents X = H, Me and OMe and M = Pd, Pt and Mn (Chart 1). The metals inserted smoothly, with standard metal salts in hot or refluxing pyridine, as expected in light of the larger $N_4$ core size of AHPs relative to corroles[12,13,14,15,16] and isocorroles.[17,18,19,20] Palladium insertion occurred fastest, reaching completion in ~3 h, while Mn and Pt insertion took ~16 h. The metal insertions could be conveniently followed visually, on account of marked changes in color of the reaction mixture, or with UV-vis-NIR absorption spectroscopy.

**(b) Spectroscopic and structural characterization.** The diamagnetic AHP derivatives (M = Pd and Pt) yielded well-resolved $^1$H NMR spectra, with the expected doubling of the number of unique $\beta$-protons relative to corroles (8 versus 4, Figure 1). Conclusive proof of structure came from two single-crystal X-ray diffraction analyses, one for free base $H_2$[Me-AHP] and one for its Pd complex Pd[Me-AHP] (Figure 2). The free-base structure exhibits the same hydrogen bonding motif and tautomer as previously observed.[5,6] Both the free-base and Pd structures are structures exhibit a nonplanar macrocycle, with the pyrrole ring attached to the 4-aminotriazole-derived nitrogen tilted relative to the mean plane of the other three pyrrole units.

Cyclic voltammetry (Figure 3) and UV-vis-NIR spectroscopy (Figure 4) afforded electronic structural insight into the compounds studied (Table 1). The free-base, Pd, and Pt AHPs were all found to exhibit two irreversible oxidations and two reversible reductions. Substituent effects of the *para* substituent X were found to be small, but as expected, with the potentials varying as H > Me > OMe. Given the focus of the present study, we have not, as of yet, attempted to understand the origin of the irreversibility of the first oxidation wave. Equating the difference between the first oxidation peak potential and the reduction potential to the electrochemical HOMO-LUMO gap, we arrive at a narrow range of values, 1.97 ± 0.05 V vs. Ag|AgCl, with the lowest values observed for the Pt-AHP derivatives.

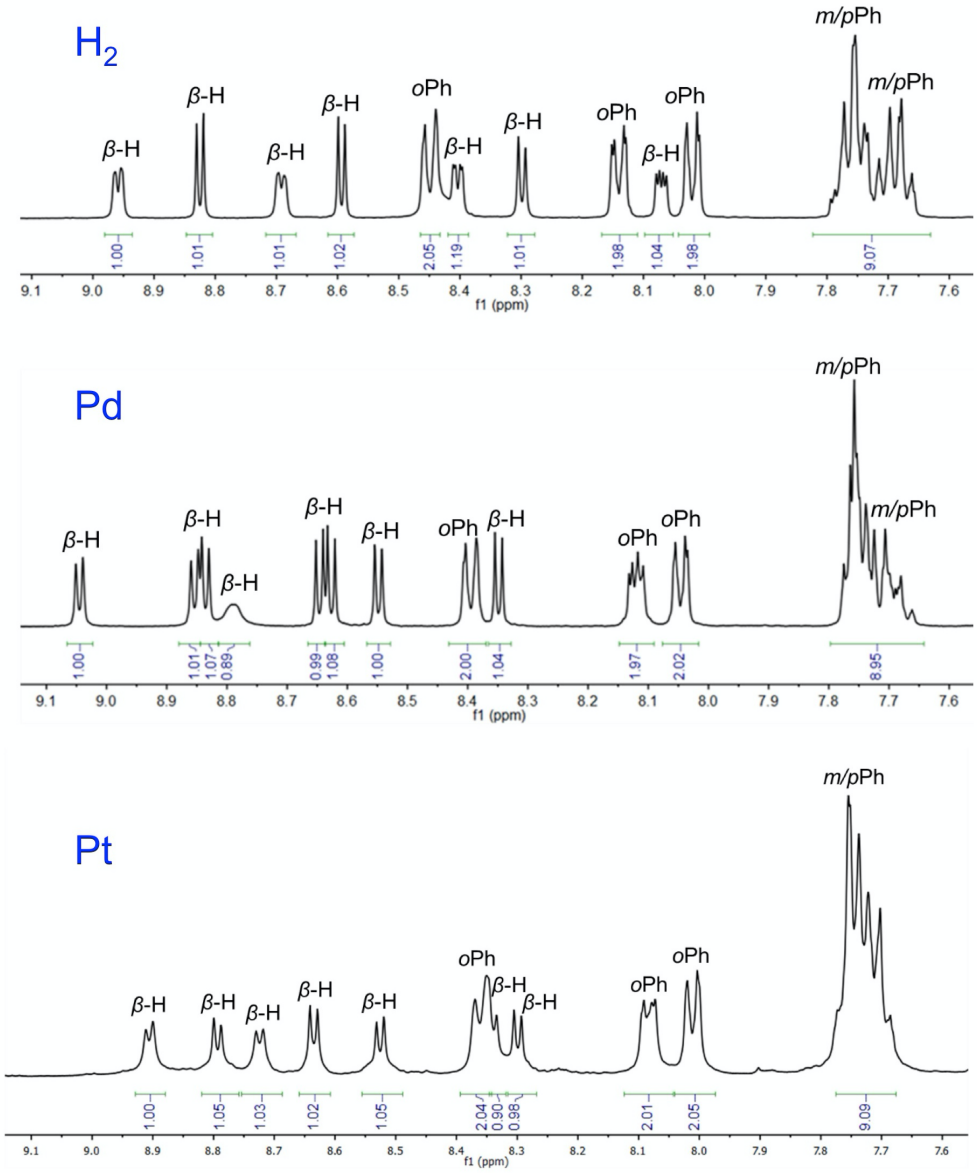


Figure 1. Aromatic regions of the $^{1}$H NMR spectra of M[H-AHP] (M = $H_2$, Pd, Pt) in $CDCl_3$.

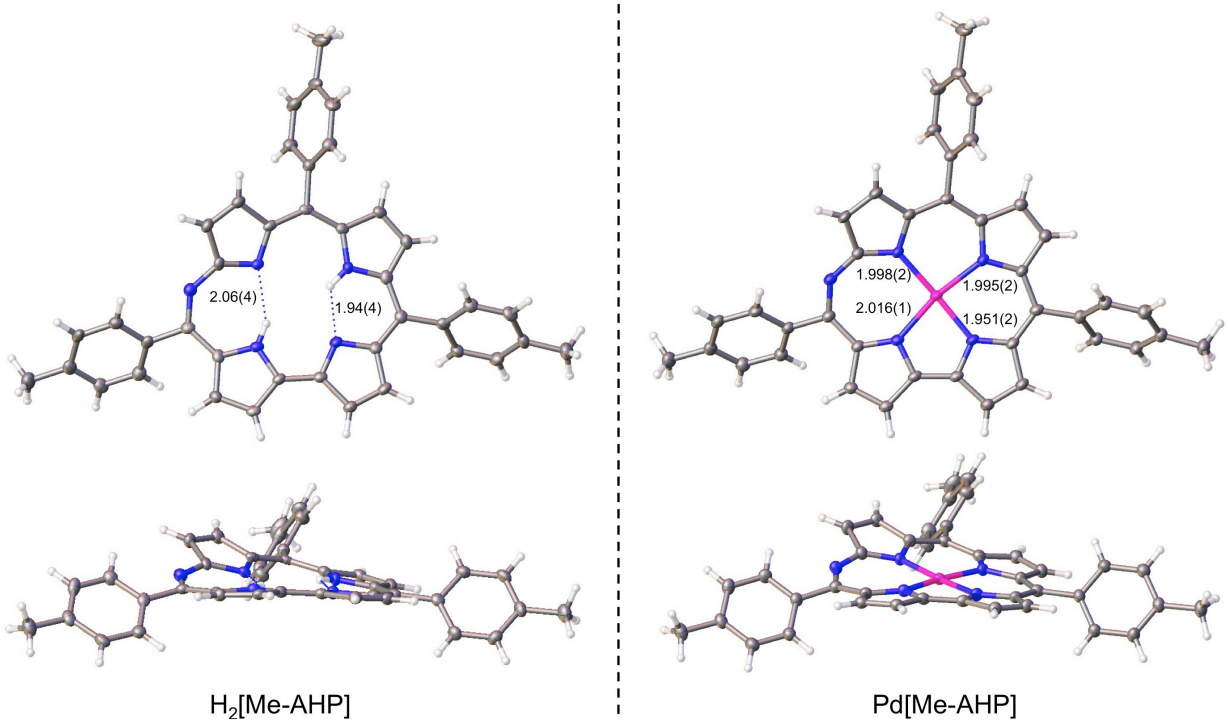


Figure 2. X-ray structures (top and side views) of $H_2$[Me-AHP] (left) and Pd[Me-AHP] (right).

The free-base AHPs exhibit sharp Soret bands and apparent three-humped Q bands. The metal complexes in contrast exhibit intricately structured Soret and Q features, as expected for a low-symmetry macrocycle. The Pd complexes exhibit strong absorption in the orange-red region of the visible spectrum (570-650 nm), while the Q bands of the Pt and Mn complexes taper off past 700 nm, i.e., in the near-infrared. The lower-energy absorption of the Pt[X-AHP] series, relative to Pd[X-AHP], is consistent with the slightly lower electrochemical HOMO-LUMO gap for the Pt series.

The luminescence properties of a set of metallo-AHP derivatives, M[Me-AHP] (M = Mn, Pd, Pt), were examined in toluene. All solutions were thoroughly deoxygenated with ultra-pure nitrogen (99.99999% purity). For all three compounds, we failed to register any emission in the red to NIR spectral range (up to 1020 nm), leading all us to conclude that the compounds are not emissive or exhibit such weak emission ($\Phi << 0.1\%$) that precludes more thorough photophysical studies.

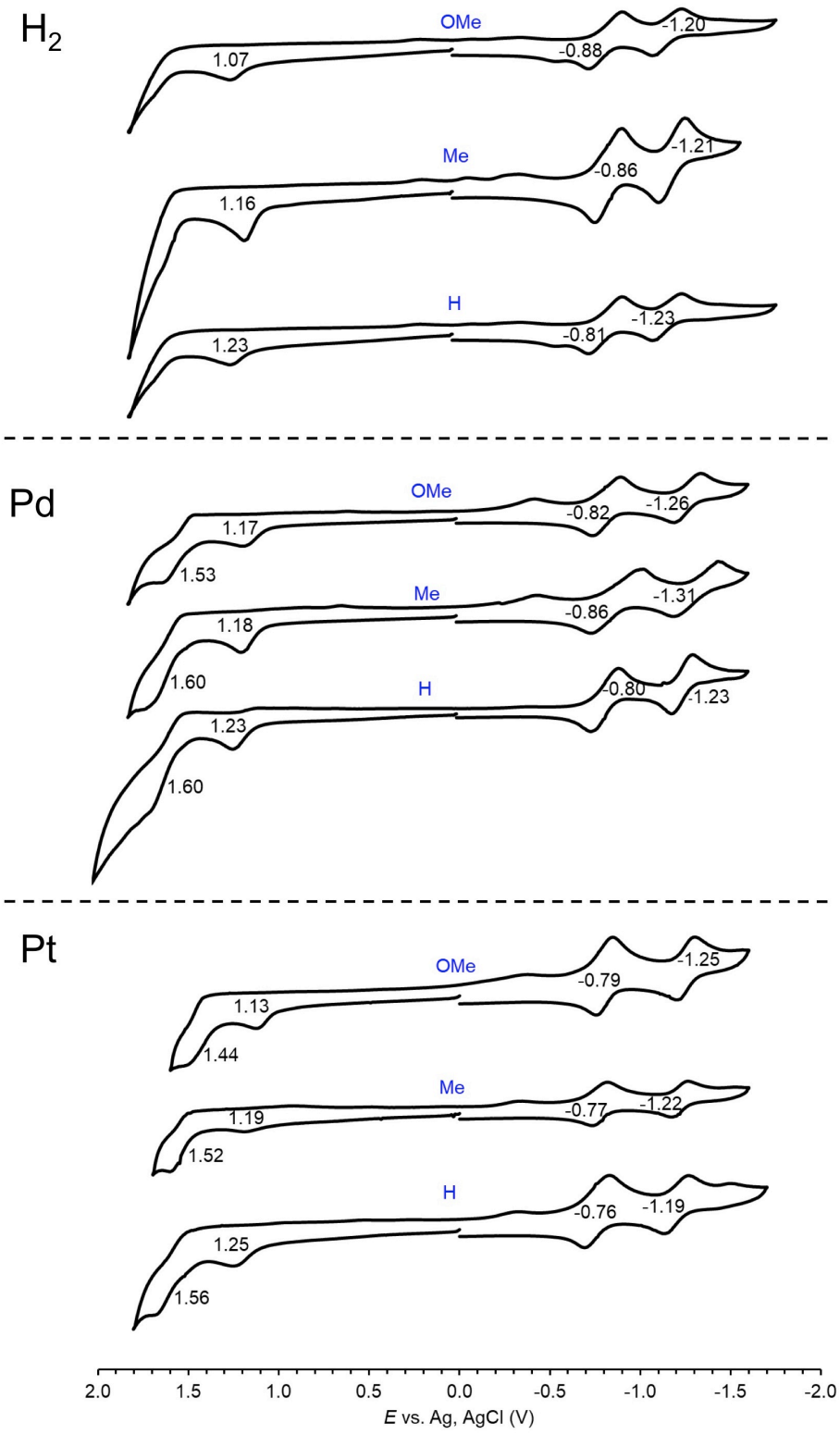


Figure 3. Cyclic voltammograms of M[X-AHP] (M = $H_2$, Pd, Pt; X = OMe, Me, H) in $CH_2Cl_2$ containing 0.1 M TBAP; scan rate 100 $mV \cdot s^{-1}$.

**Table 1.** Selected UV-vis (nm) and electrochemical (V vs. Ag|AgCl) data for M[X-AHP] (M = $H_2$, Pd, Pt).

| Compound | *Soret band* | *Q-band* | $E'_{ox2}$ | $E'_{ox1}$ | $E_{1/2red1}$ | $E_{1/2red2}$ |
|---|---|---|---|---|---|---|
| $H_2$[H-AHP] | 412 | 570 | - | 1.23 | -0.81 | -1.23 |
| $H_2$[Me-AHP] | 417 | 571 | - | 1.16 | -0.86 | -1.21 |
| $H_2$[OMe-AHP] | 423 | 574 | - | 1.07 | -0.88 | -1.20 |
| Pd[H-AHP] | 378,398,416,439,464 | 591,625 | 1.60 | 1.23 | -0.80 | -1.23 |
| Pd[Me-AHP] | 383,402,415,439,466 | 593,627 | 1.60 | 1.18 | -0.86 | -1.31 |
| Pd[OMe-AHP] | 384,420,443,468 | 596,629 | 1.53 | 1.17 | -0.82 | -1.26 |
| Pt[H-AHP] | 383398,462 | 585,627,672 | 1.56 | 1.25 | -0.76 | -1.19 |
| Pt[Me-AHP] | 386,397,465 | 585,627,672 | 1.52 | 1.19 | -0.77 | -1.22 |
| Pt[OMe-AHP] | 398,465 | 585,627,674 | 1.44 | 1.13 | -0.79 | -1.25 |

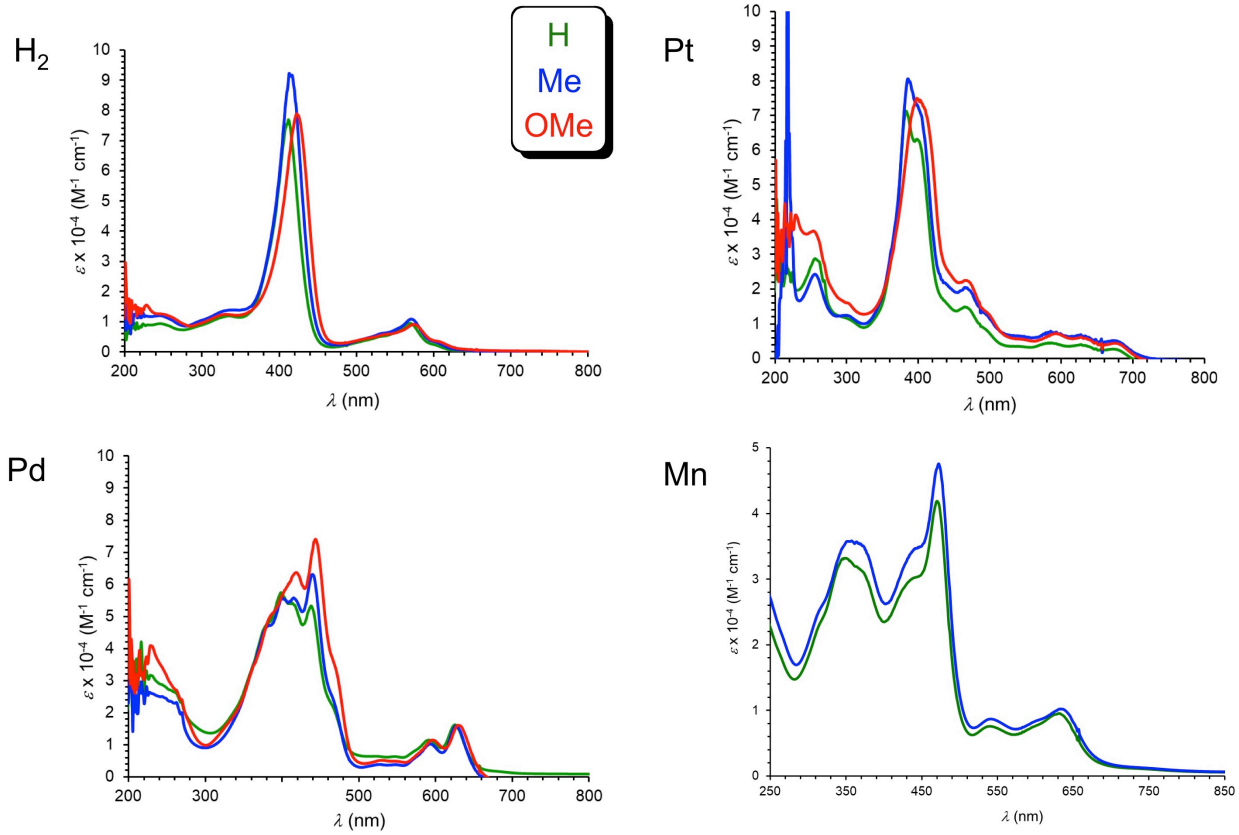


Figure 4. UV-vis-NIR spectra of for M[X-AHP] (M = $H_2$, Pd, Pt, Mn) in dichloromethane. The spectra are color-coded for the *para* substituent X.

**(c) Singlet oxygen sensitization**. Singlet oxygen quantum yields were determined as previously described.[21] The assay relies on the singlet oxygen acceptor 9,10-dimethylanthracene, whose characteristic UV absorption vanishes upon reaction with $^1O_2$. Methylene blue, with $\Phi(^1O_2) = 0.48$, was used as the standard. Figure 5 depicts the bleaching of 9,10-dimethylanthracene at 358 nm in presence of M[Me-AHP] (M = Mn, Pd, Pt), with the corresponding absorption spectra included as Supporting Information. It should be noted that both 9,10-dimethylanthracene and the AHP photosensitizer absorb at 358nm, where both 9,10-demethylanthracene and the photosensitizer absorb light; however, since no degradation of the photosensitizer was observed throughout the experiment (Figures S21-24), the spectral changes can be attributed solely to the bleaching of 9,10-dimethylanthracene. As can be seen, both the Pd(II) and Pt(II) complexes generate singlet oxygen, whereas no bleaching of dimethylanthracene was observed for Mn[Me-AHP], i.e., the $\Phi(^1O_2)$ is essentially 0. The Pd(II) complex was found to be a very efficient photosensitizer with $\Phi(^1O_2)$ of = 0.84 ± 0.02 (average of 3 assays) in 9:1 v/v ethanol:tetrahydrofuran, which compares favorably with the best singlet oxygen quantum yields measured for 5d metallocorroles.[22,23,24,25,26] On the other hand, the $\Phi(^1O_2)$ for Pt[Me-AHP] was found to be only 0.11 ± 0.01. Since none of the complexes was found to exhibit room-temperature phosphorescence in the 600-1020 nm range, transient absorption spectroscopy was carried out to shed light on the mechanism of singlet oxygen sensitization.

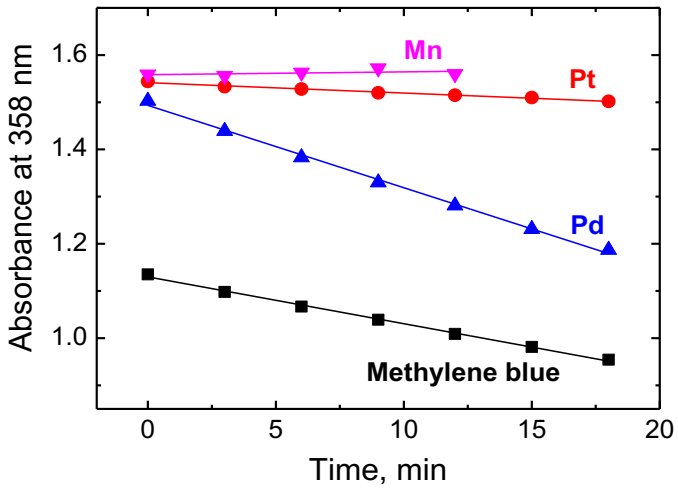


Figure 5. Bleaching of 9,10-dimethylanthracene upon reaction with $^1O_2$ photosensitized by M[Me-AHP] (M = Mn, Pd, Pt) and the standard – methylene blue. Note that the absorbance at 358 nm represents the combined absorbance of 9,10-dimethylanthracene and the photosensitizer that does not bleach (see Figures S21-S24). All the compounds showed identical absorbance at irradiation wavelength (580 nm).

**(d) Transient absorption (TA) apectroscopy.** As shown in Figure 6, Irradiation of the solution of Pd[Me-AHP] in deoxygenated 9:1 v/v ethanol/tetrahydrofuran with 532-nm laser light results in distinct absorption changes (Figure 6A). These characteristic changes correspond to bleaching of the ground state spectrum (Figure 6A) upon population of the triplet state. Additionally, new, strong absorption centered at ~500 nm emerges along with a weaker peak at ~680 nm. The positive peaks are attributed to absorption of the species in the triplet state. The time traces revealed mono-exponential decay (Figure 6B). Fitting the time traces resulted in identical triplet lifetimes, $\tau_T = 3.6 \pm 0.4$ µs, for all the investigated wavelengths.

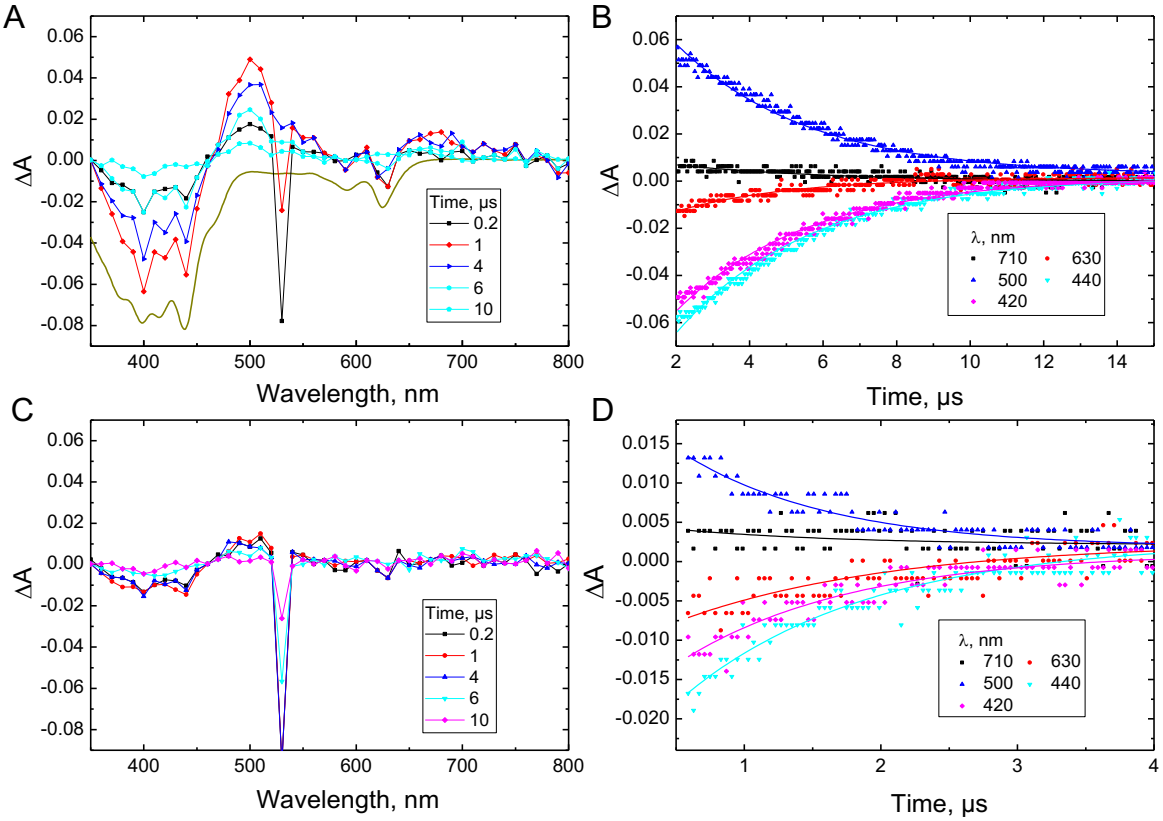


Figure 6. Transient absorption spectra (A, C) for the deoxygenenated (A) and air-saturated (C) solutions of Pd[Me-AHP] in 9:1 v/v ethanol/tetrahydrofuran upon excitation at 532 nm. The gray line in A shows UV-vis-NIR absorption spectrum of Pd[Me-AHP] under the same conditions. Panels B and D: time traces for selected wavelengths for deoxygenated (B) and air-saturated (D) solutions. Symbols are experimental data; solid lines are fits according to the monoexponential decay model.

Upon saturation with air, the intensity of all optical traces decreased significantly (~3-4 fold), indicating triplet state quenching by dioxygen (Figure 6C). Fitting of the time traces (Figure 6D) resulted in $\tau_T = 1.4 \pm 0.1$ µs under these experimental conditions. Analogous

measurements were also conducted for Pd[Me-AHP] in toluene (Figure S25). The transient absorption spectra proved very similar to those obtained in 9:1 v/v ethanol/tetrahydrofuran. Triplet lifetimes of 3.8 ± 0.4 μs and 1.6 ± 0.2 μs were obtained under deoxygenated and air-saturated conditions, respectively, suggesting that solvent polarity does not significantly affect the excited-state properties.

Excitation of Pt[Me-AHP] was performed at 355 nm due to the comparably low absorption at 532 nm. The changes in absorption upon excitation were found to be rather small (Figure 7), indicating much less efficient population of the triplet state. As expected, the observed changes were consistent with the shape of the ground-state absorption spectrum. The triplet decay time extracted by fitting the time trace at 400 nm was found to be 1.3 ± 0.1 μs, which is significantly lower than in case of Pd[Me-AHP]. Although noticeable reduction in ground-state bleaching was observed upon addition of air (Figure S26), we were not able to reliably determine $\tau_T$ in these conditions due to low intensity of the signals. Like its Pd counterpart, Pt[Me-AHP] in toluene (Figure S27) showed excited-state characteristics similar to those in 9:1 v/v ethanol/tetrahydrofuran, with $\tau_T$ = 1.4 ± 0.1 μs under anoxic conditions.

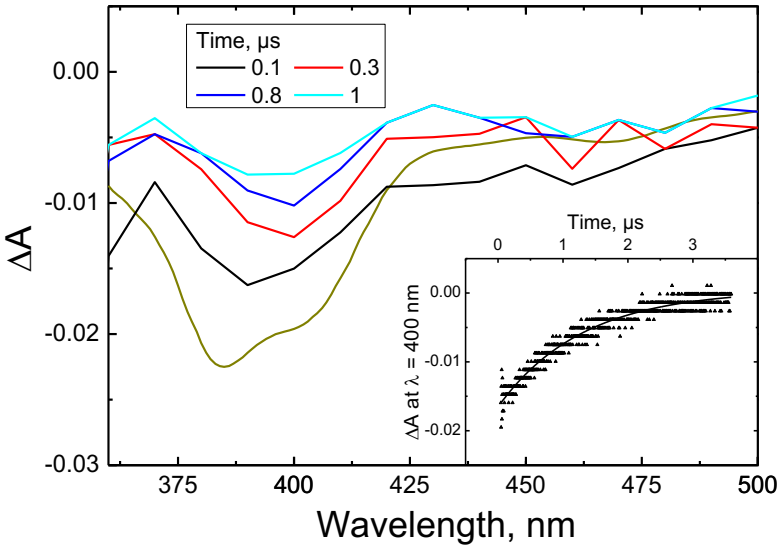


Figure 7. Transient absorption spectra for the deoxygenenated solution of Pt[Me-AHP] in 9:1 v/v ethanol/tetrahydrofuran upon excitation at 355 nm. Gray line shows UV-Vis absorption spectrum of Pt[Me-AHP] in the same conditions. The inset shows the time trace obtained at 400 nm. Symbols are experimental data; the solid line is the fit according to the monoexponential decay model.

Finally, we investigated the behaviour of Mn[Me-AHP] in the same conditions. No ground state bleaching or appearance of new absorption was detected upon excitation of deoxygenated solutions of the complex in 9:1 v/v ethanol/tetrahydrofuran or toluene (Figure S28).

## CONCLUSION

In conclusion, although the transition metal azahemiporphycenes studies have proved nonemissive, they vary widely in terms of their ability to sensitize singlet oxygen. Thus, Pd[Me-AHP] was found to exhibit a singlet oxygen quantum yield of 84%, while the corresponding value for Pt[Me-AHP] is 11%. In contrast, Mn[Me-AHP] does not sensitize singlet oxygen at all. The excellent performance of Pd[Me-AHP] could be rationalized via transient absorption spectroscopy, which revealed substantial population of the triplet state, while such populations were found to be much lower and essentially zero for Pt and Mn, respectively. By virtue of their strong absorption in the red and high singlet oxygen-sensitizing ability, palladium azahemiporphycenes appear to exhibit considerable promise as a new class of triplet photosensitizers for photodynamic therapy.

## Experimental details

**General procedure for the synthesis of free-base 6-azahemiporphycenes, $H_2$[X-AHP], where X = H, Me and OMe.** To a 100-mL round-bottom flask equipped with a stirring bar were added free-base corrole $H_3$[T*p*XPC] (0.1355 mmol) and DDQ (0.1355 mmol) and the mixture was dissolved in dichloromethane (20 mL). Upon stirring for 10 min at room temperature, 4-aminotriazole (5 equiv, 0.6778 mmol, dissolved in 1 mL DMSO) and KOH (200 mg) were added, and the reaction mixture was stirred overnight at room temperature. At that point, the reaction was judged complete, based on HRMS and UV-vis-NIR analyses of the reaction mixture. Distilled water (20 mL) was added and the reaction mixture was stirred for 1 h to transfer the DDQ to the aqueous phase. The organic phase was separated and washed with water (20 mL x 2). The purple organic phase containing the product was then dried over anhydrous sodium sulfate, the solvent was removed by rotary evaporation, and the residue was purified via column chromatography a silica gel column using 3:2 hexane/dichloromethane as the mobile phase. The eluate, upon rotary evaporation, yielded the desired product as a purple solid in 49 to 68 % yield. Analytical data for $H_2$[X-AHP], where X = H, Me and OMe, are as follows.

**$H_2$[H-AHP]**. Yield 43 mg (58.8%). UV-vis ($CH_2Cl_2$) $\lambda_{max}$ [nm, ε x $10^{-4}$ ($M^{-1}cm^{-1}$)]: 412 (7.70), 570 (0.95). $^1$H NMR (400 MHz, 25 °C ): δ 8.95 (d, 1H, $^3J_{HH}$ = 3.56 Hz, *β*-H); 8.82 (d, 1H, $^3J_{HH}$ = 4.44 Hz, *β*-H); 8.69 (d, 1H, $^3J_{HH}$ = 3.56 Hz, *β*-H); 8.59 (d, 1H, $^3J_{HH}$ = 4.44 Hz, *β*-H ); 8.45 (d, 2H, $^3J_{HH}$ = 7.12 Hz, *o*Ph); 8.40 (d, 1H, $^3J_{HH}$ = 5.96 Hz, *β*-H); 8.29 (d, 1H, $^3J_{HH}$ = 4.52 Hz, *β*-H); 8.13 (d, 2H, $^3J_{HH}$ = 7.76 Hz, *o*Ph); 8.07 (d, 1H, $^3J_{HH}$ = 5.28 Hz, *β*-H); 8.01 (d, 2H, $^3J_{HH}$ = 8.12 Hz, *o*Ph), 7.79—7.65 (m, 9H, Ph). MS (ESI) [$M^+$] = 540.2183 (expt), 540.2183 (calcd for $C_{37}H_{26}N_5$).

**$H_2$[Me-AHP]**. Yield 53.7 mg (68%). UV-vis ($CH_2Cl_2$) $\lambda_{max}$ [nm, ε x $10^{-4}$ ($M^{-1}cm^{-1}$)]: 417 (9.17), 571 (1.08). $^1$H NMR (400 MHz, 25 °C ): δ 8.91 (d, 1H, $^3J_{HH}$ = 3.84 Hz, *β*-H); 8.72 (d, 1H, $^3J_{HH}$ = 4.40 Hz, *β*-H); 8.66 (d, 1H, $^3J_{HH}$ = 4.32 Hz, *β*-H); 8.57 (d, 1H, $^3J_{HH}$ = 4.40 Hz, *β*-H ); 8.37 (d, 1H, $^3J_{HH}$ = 4.92 Hz, *β-H*); 8.34 (d, 2H, $^3J_{HH}$ = 7.88 Hz, *o*Ph); 8.26 (d, 1H, $^3J_{HH}$ = 4.48 Hz, *β*-H); 8.05 (d, 1H, $^3J_{HH}$ = 4.92 Hz, *β-H*); 8.02 (d, 2H, $^3J_{HH}$ =7.88 Hz, *o*Ph); 7.88 (d, 2H, $^3J_{HH}$ = 7,72 Hz, *o*Ph), 7.57 (d, 2H, $^3J_{HH}$ = 7.44 Hz, *m*Ph); 7.56 (d, 2H, $^3J_{HH}$ = 7.24 Hz, *m*Ph); 7.47 (d, 2H, $^3J_{HH}$ = 7.76 Hz, *m*Ph); 2.65 (s, 3H, *p*CH3); 2.64 (s, 3H, *p*$CH_3$); 2.60 (s, 3H, *p*$CH_3$). MS (ESI) [$M^+$] = 582.2653 (expt), 582.2652 (calcd for $C_{40}H_{32}N_5$).

**$H_2$[OMe-AHP]**. Yield 41.8 mg (49%). UV-vis ($CH_2Cl_2$) $\lambda_{max}$ [nm, ε x $10^{-4}$ ($M^{-1}cm^{-1}$)]: 423 (7.89), 574 (0.91). $^1$H NMR (400 MHz, 25 °C ): δ 8.83 (d, 1H, $^3J_{HH}$ = 4.00 Hz, *β*-H); 8.70 (d, 1H, $^3J_{HH}$ = 4.20 Hz, *β*-H); 8.66 (bs, 1H, *β*-H); 8.51 (d, 1H, $^3J_{HH}$ = 4.20 Hz, *β*-H ); 8.40 (d, 2H, $^3J_{HH}$ = 8.20 Hz, *o*Ph); 8.34 (d, 1H, $^3J_{HH}$ = 3.40 Hz, *β*-H); 8.21 (bs, 1H, *β*-H); 8.05 (d, 2H, $^3J_{HH}$ = 8,02 Hz, *o*Ph); 8.02 (bs, 1H, *β*-H); 7.90 (d, 2H, $^3J_{HH}$ = 8.16 Hz, *o*Ph), 7.30 (d, 2H, $^3J_{HH}$ = 6.88 Hz, *m*Ph); 7.28 (d, 2H, $^3J_{HH}$ = 7.68 Hz, *m*Ph); 7.20 (d, 2H, $^3J_{HH}$ = 8.24 Hz, *m*Ph); 4.06 (s, 3H, *p*OCH3); 4.05 (s, 3H, *p*$OCH_3$); 4.02 (s, 3H, *p*$OCH_3$). MS (ESI) [$M^+$] = 630.2499(expt), 630.2500 (calcd for $C_{40}H_{32}N_5O_3$).

**General procedure for the synthesis of Pd[X-AHP], where X = H, Me and OMe.** To a 50-mL of round-bottom flask equipped with a strirring bar were added free-base $H_2$[X-AHP] (0.092 mmol), palladium(II) acetate (3 equiv), and pyridine (10 mL). The mixture was heated at 100 °C under stirring for 3h, in the course of which the purple color of the starting material was gradually replaced by the deep green color of the Pd complex. The reaction mixture was cooled to room temperature and the solvent removed by rotary evaporation. The crude product thus obtained was subjected to column chromatography on a silica gel colunm and 2:1 (v/v) *n*-

hexane/dichloromethane as the mobile phase, resulting in the desired deep-green product in 79 to 85 % yield.

**Pd[H-AHP]**. Yield 47.4 mg (79.5%). UV-vis ($CH_2Cl_2$) $\lambda_{max}$ [nm, ε x $10^{-4}$ ($M^{-1}cm^{-1}$)]: 398 (5.74), 438(5.33), 591 (1.14), 625 (1.62). $^1$H NMR (400 MHz, 25 °C ): δ 9.04 (d, 1H, $^3J_{HH}$ = 4.60 Hz, *β*-H); 8.85 (d, 1H, $^3J_{HH}$ = 4.76 Hz, *β*-H); 8.53 (d, 1H, $^3J_{HH}$ = 4.64 Hz, *β*-H); 8.78 (s, 1H, *β*-H ); 8.64 (d, 1H, $^3J_{HH}$ = 4.76 Hz, *β*-H); 8.62 (d, 1H, $^3J_{HH}$ = 4.84 Hz, *β*-H); 8.54 (d, 1H, $^3J_{HH}$ = 4.68 Hz, *β*-H); 8.39 (d, 2H, $^3J_{HH}$ = 7.08 Hz, *o*Ph); 8.34 (d, 1H, $^3J_{HH}$ = 4.76 Hz, *β*-H); 8.11 (d, 2H, $^3J_{HH}$ = 7.20 Hz, *o*Ph); 8.04 (d, 2H, $^3J_{HH}$ = 6.44 Hz, *o*Ph); 7.78—7.65 (m, 9H, Ph). MS (ESI) [$M^+$] = 644.1075 (expt), 644.1075 (calcd for $C_{37}H_{24}N_5Pd$).

**Pd[Me-AHP]**. Yield 52 mg (81.85%). UV-vis ($CH_2Cl_2$) $\lambda_{max}$ [nm, ε x $10^{-4}$ ($M^{-1}cm^{-1}$)]: 401 (5.54), 415(5.57), 439 (6.20), 593 (1.02), 627 (1.58). $^1$H NMR (400 MHz, 25 °C ): δ 8.90 (s, 1H, *β*-H); 8,76 (d, 1H, $^3J_{HH}$ = 4.32 Hz, *β*-H); 8.71 (s, 1H, *β*-H); 8.61 (d, 1H, $^3J_{HH}$ = 4.76 Hz *β*-H ); 8.59 (d, 1H, $^3J_{HH}$ = 4.84 Hz, *β*-H); 8.47 (d, 1H, $^3J_{HH}$ = 4.84 Hz, *β*-H); 8.32 (d, 1H, $^3J_{HH}$ = 4.72 Hz, *β*-H); 8.24 (d, 2H, $^3J_{HH}$ = 7.32 Hz, *o*Ph); 7.95 (d, 2H, $^3J_{HH}$ = 7.68 Hz, Ph); 7.88 (d, 2H, $^3J_{HH}$ = 7.76 Hz, *o*Ph); 7.55 (d, 2H,$^3J_{HH}$ = 7.68 Hz, *m*Ph); 7.54 (d, 2H, $^3J_{HH}$ = 7.68 Hz, *m*Ph); 7.50 (d, 2H, $^3J_{HH}$ = 7.72 Hz, *m*Ph); 2.67 (s, 6H, *p*$CH_3$); 2.63 (s, 3H, *p*$CH_3$). MS (ESI) [$M^+$] = 686.1550 (expt), 686.1545 (calcd for $C_{40}H_{30}N_5Pd$).

**Pd[OMe-AHP]**. Yield 58.2 mg (85.63%). UV-vis ($CH_2Cl_2$) $\lambda_{max}$ [nm, ε x $10^{-4}$ ($M^{-1}cm^{-1}$)]: 418 (6.36), 443(7.40), 496 (1.14), 629 (1.60). $^1$H NMR (400 MHz, 25°C ): δ 8.81 (bs, 1H, *β*-H); 8,68 (bs, 1H, *β*-H); 8.62 (bs, 1H, *β*-H); 8.57 (d, 1H, $^3J_{HH}$ = 4.64 Hz, *β*-H ); 8.55 (d, 1H, $^3J_{HH}$ = 4.88 Hz, *β*-H); 8.41 (bs, 1H, *β*-H); 8.28 (d, 2H, $^3J_{HH}$ = 7.72 Hz, *o*Ph); 8.27 (bs, 1H, *β*-H); 7.96 (d, 2H, $^3J_{HH}$ = 8.12 Hz, *o*Ph); 7.88 (d, 2H, $^3J_{HH}$ = 8.36 Hz, *o*Ph) ); 7.29 (d, 2H, $^3J_{HH}$ = 8.60 Hz, *m*Ph) ); 7.28 (d, 2H, $^3J_{HH}$ = 8.60 Hz, *m*Ph) ); 7.23 (d, 2H, $^3J_{HH}$ = 8.52 Hz, *m*Ph) ); 4.06 (s, 6H, *p*$OCH_3$) ); 4.04 (s, 3H, *p*$OCH_3$). MS (ESI) [$M^+$] = 734.1399 (expt), 734.1392 (calcd for $C_{40}H_{30}N_5O_3Pd$).

**General procedure for the syntheses of Pt[X-AHP], where X = H, Me and OMe.** To a 50-mL of round-bottom flask equipped with a strirring bar was added free-base $H_2$[X-AHP] (0.074 mmol), platinum(II) chloride (3 equiv, 0.222 mmol), and pyridine (10 mL). The mixture was refluxed under stirring for 16 h. Th, in the course of which the purple color of the starting material was replaced by the yellowish-green color of the platinum complex, with a hypsochromically shifted Soret band. The reaction mixture was cooled to room temperature and the solvent removed by rotary evaporation. The crude product thus obtained was subjected to

column chromatography on a silica gel colunm and 3:2 (v/v) *n*-hexane/dichloromethane as the mobile phase, resulting in the desired yellowish-green product in 64 to 67 % yield.

**Pt[H-AHP]**. Yield 36,3 mg (67%). UV-vis ($CH_2Cl_2$) $\lambda_{max}$ [nm, ε x $10^{-4}$ ($M^{-1}cm^{-1}$)]: 383 (7.12), 398 (6.32), 462 (1.45), 585 (0.46), 627 (0.41), 672 (0.28). $^1$H NMR (400 MHz, 25°C ): δ 8.90 (d, 1H, $^3J_{HH}$ = 4.60 Hz, *β*-H); 8.79 (d, 1H, $^3J_{HH}$ = 4.72 Hz, *β*-H); 8.72 (d, 1H, $^3J_{HH}$ = 4.56 Hz, *β*-H); 8.63 (d, 1H, $^3J_{HH}$ = 4.96 Hz *β*-H ); 8.52 (d, 1H, $^3J_{HH}$ = 4.84 Hz, *β*-H); 8.36 (d, 2H, $^3J_{HH}$ = 7.52 Hz, *o*Ph); 8.33 (d, 1H, $^3J_{HH}$ = 3.56 Hz, *β*-H); 8.29 (d, 1H, $^3J_{HH}$ = 4.84 Hz, *β*-H); 8.02 (d, 2H, $^3J_{HH}$ = 7.44 Hz, *o*Ph); 8.01 (d, 2H, $^3J_{HH}$ = 6.64 Hz, *o*Ph); 7.78—7.67 (m, 9H, Ph). MS (ESI) [$M^+$] = 733.1686 (expt), 733.1677 (calcd for $C_{37}H_{24}N_5Pt$).

**Pt[Me-AHP]**. Yield 37.8 mg (66%). UV-vis ($CH_2Cl_2$) $\lambda_{max}$ [nm, ε x $10^{-4}$ ($M^{-1}cm^{-1}$)]: 386 (8.05), 397 (7.36), 465 (2.05), 585 (0.79), 627 (0.69), 672 (0.52). $^1$H NMR (400 MHz, 25 °C ): δ 8.93 (d, 1H, $^3J_{HH}$ = 4.64 Hz, *β*-H); 8,83 (d, 1H, $^3J_{HH}$ = 4.72 Hz, *β*-H); 8.75 (d, 1H, $^3J_{HH}$ = 4.76 Hz, *β*-H); 8.64 (d, 1H, $^3J_{HH}$ = 4.88 Hz *β*-H ); 8.53 (d, 1H, $^3J_{HH}$ = 4.88 Hz, *β*-H); 8.37 (d, 1H, $^3J_{HH}$ = 4.76 Hz, *β*-H); 8.30 (d, 1H, $^3J_{HH}$ = 4.84 Hz, *β*-H); 8.26 (d, 2H,$^3J_{HH}$ = 7.40 Hz, *o*Ph); 7.98 (d, 2H, $^3J_{HH}$ = 7.84 Hz, *o*Ph); 7.89 (d, 2H, $^3J_{HH}$ = 7.80 Hz, *o*Ph); 7.56 (d, 2H, $^3J_{HH}$ = 5.68 Hz, *m*Ph); 7.54 (d, 2H, $^3J_{HH}$ = 7.52 Hz, *m*Ph); 7.50 (d, 2H, $^3J_{HH}$ = 7.76 Hz, *m*Ph); 2.66 (s, 6H, *p*$CH_3$); 2.62 (s, 3H, *p*$CH_3$). MS (ESI) [$M^+$] = 775.2156 (expt), 775.2147 (calcd for $C_{40}H_{30}N_5Pt$).

**Pt[OMe-AHP]**. Yield 38.9 mg (64%). UV-vis ($CH_2Cl_2$) $\lambda_{max}$ [nm, ε x $10^{-4}$ ($M^{-1}cm^{-1}$)]: 398 (8.05), 465 (2.25), 585 (0.70), 627 (0.63), 674 (0.44). $^1$H NMR (400 MHz, 25 °C ): δ 8.94 (d, 1H, $^3J_{HH}$ = 4.60 Hz, *β*-H); 8,83 (d, 1H, $^3J_{HH}$ = 4.64 Hz, *β*-H); 8.75 (d, 1H, $^3J_{HH}$ = 4.68 Hz, *β*-H); 8.63 (d, 1H, $^3J_{HH}$ = 4.76 Hz *β*-H ); 8.53 (d, 1H, $^3J_{HH}$ = 4.84 Hz, *β*-H); 8.37 (d, 1H, $^3J_{HH}$ = 4.64 Hz, *β*-H); 8.36 (d, 2H, $^3J_{HH}$ = 8.80 Hz, *o*Ph); 8.31 (d, 1H,$^3J_{HH}$ = 4.80 Hz, *β*-H); 8.02 (d, 2H, $^3J_{HH}$ = 8.44 Hz, *o*Ph); 7.92 (d, 2H, $^3J_{HH}$ = 8.36 Hz, *o*Ph); 7.29 (d, 2H, $^3J_{HH}$ = 8.44 Hz, *m*Ph); 7.27 (d, 2H, $^3J_{HH}$ = 8.44 Hz, *m*Ph); 7.23 (d, 2H, $^3J_{HH}$ = 12.48 Hz, *m*Ph); 4.06 (s, 6H, *p*$OCH_3$); 4.03 (s, 3H, *p*$OCH_3$). MS (ESI) [$M^+$] = 823.2009 (expt), 823.1994 (calcd for $C_{40}H_{30}N_5O_3Pt$).

**X-ray diffraction analyses**. Crystallographic-quality crystals of both $H_2$[Me-AHP] and Pd[Me-AHP] were obtained by slow evaporation of concentrated solutions of the compounds in dichloromethane-methanol. Samples were mounted on MiTeGen® kapton loops and placed in a nitrogen cold streams on the goniometer head of Bruker D8 diffractometers. For Pd[Me-AHP], the analysis was performed with data collected on beamline 11.3.1 at the Advanced Light Source at the Lawrence Berkeley National Laboratory using synchrotron radiation monochromated with silicon(111) to a wavelength of 0.7293(1)Å. The structure was solved by direct methods

(SHELXT) and refined by full-matrix least squares on $F^2$ (SHELXL-2013). All non-hydrogen atoms were refined anisotropically. Hydrogen atoms were geometrically calculated and refined as riding atoms. Full details of the analyses are given in the CIF files available from the Cambridge Structural Database.

**Selected crystal Data for $H_2$[Me-AHP]**. Chemical formula $C_{40}H_{31}N_5$, $M_r$ = 581.70, orthorhombic, *Pbca*, a = 19.2471(5) Å, b = 11.2754(3) Å, c = 27.7016(7) Å, $\alpha = \beta = \gamma = 90^\circ$, $V$ = 6011.8(3) Å$^3$, $T$ = 126.0(1) K, $Z$ = 8, $Z'$ = 1, $\mu$(Cu K$_\alpha$) = 0.596, 44172 reflections measured, 5312 unique ($R_{int}$ = 0.0670) which were used in all calculations. The final $wR_2$ was 0.1669 (all data) and $R_1$ was 0.0858 [$I \geq 2\ \sigma(I)$].

**Selected crystal Data for Pd[Me-AHP]**. Chemical formula $C_{40}H_{20}N_5Pd$, $M_r$ = 686.08, orthorhombic, *Pbca*, a = 19.3019(8) Å, b = 11.2284(5) Å, c = 27.6885(12) Å, $\alpha = \beta = \gamma = 90^\circ$, $V$ = 6000.9(4) Å$^3$, $T$ = 100(2) K, $Z$ = 8, $Z'$ = 1, $\lambda$ 0.7293 Å, 63273 reflections measured, 11427 unique ($R_{int}$ = 0.0645) which were used in all calculations. The final $wR_2$ was 0.1255 (all data) and $R_1$ was 0.0506 [$I \geq 2\ \sigma(I)$].

**X-ray crystallographic analysis of Pd[Me-AHP]**. The analysis was performed with data collected on beamline 11.3.1 at the Advanced Light Source at the Lawrence Berkeley National Laboratory. Samples were mounted on MiTeGen® kapton loops and placed in a 100(2) K nitrogen cold stream provided by an Oxford Cryostream 700 Plus low temperature apparatus on the goniometer head of a Bruker D8 diffractometer equipped with an APEXII CCD detector. Diffraction data were collected using synchrotron radiation monochromated using silicon(111) to a wavelength of 0.7293(1)Å. An approximate full-sphere of data was collected using 0.6° $\omega$ scans. The structure was solved by direct methods (SHELXT) and refined by full-matrix least squares on $F^2$ (SHELXL-2013). All non-hydrogen atoms were refined anisotropically. Hydrogen atoms were geometrically calculated and refined as riding atoms. Full details of the analyses are given in the crystallographic information files, which can be obtained free of charge from The Cambridge Crystallographic Data Centre via www.ccdc.cam.ac.uk/data_request/cif.

**Photophysical studies.** Screening of the azahemiporphycenes for luminescent properties was done on a Fluorolog 3 fluorescence spectrometer from Horiba (Japan) equipped with a NIR-sensitive photomultiplier R2658 from Hamamatsu (Japan). Prior to measurements, toluene solutions of the complexes in a sealable quartz cell (Hellma Analytics, Germany) were

deoxygenated by bubbling high purity nitrogen (99.99999%, Linde Gas, Austria) for at least 15 min.

TA experiments were performed on a LKS80 spectrometer (Applied Photophysics). Excitation of the samples was carried out with the light of either a frequency double (532nm, 8 ns pulse duration; 30 mJ/pulse energy) or frequency triple (355nm, 8 ns pulse duration; 15 mJ/pulse energy) Spitlight Compact 100 (Innolas) Nd:YAG laser.

## ASSOCIATED CONTENT

**Supporting Information.** $^{1}$H NMR and electrospray ionization mass spectra; spectra associated photophysical studies.

**Accession codes**. The crystal structures reported in this paper have been deposited at the Cambridge Crystallographic Data Centre and assigned the deposition numbers CCDC 2255991 and 1002323.

## Author Information


### Corresponding authors

Sergey M. Borisov: sergey.borisov@tugraz.at

Abhik Ghosh (corresponding author): abhik.ghosh@uit.no

### Other authors

Abraham B. Alemayehu: abraham.alemayehu@uit.no

Kevin J. Gagnon: kjgagnonlbl@gmail.com

Yoann Rousselin: Yoann.Rousselin@u-bourgogne.fr

Max Schmallegger: schmallegger@tugraz.at


**Notes:** The authors declare no competing financial interests.

**References**


[1] Barata, J. F.; Neves, M. G. P.; Faustino, M. A. F.; Tomé, A. C.; Cavaleiro, J. A. Strategies for corrole functionalization. *Chem. Rev.* **2017**, *117*, 3192-3253.

[2] Hiroto, S.; Miyake, Y.; Shinokubo, H. Synthesis and functionalization of porphyrins through organometallic methodologies. **2017**, *117,* 2910-3043.

[3] Szyszko, B.; Latos-Grażyński, L. Core chemistry and skeletal rearrangements of porphyrinoids and metalloporphyrinoids. *Chem. Soc. Rev.* **2015**, *44*, 3588-3616.

[4] Matano, Y. Synthesis of aza-, oxa-, and thiaporphyrins and related compounds. *Chem. Rev.* **2017**, *117*, 3138-3191.

[5] Mandoj, F.; Stefanelli, M.; Nardis, S.; Mastroianni, M.; Fronczek, F. R.; Smith, K. M.; Paolesse, R. 6-Azahemiporphycene: a further example of corrole metamorphosis. *Chem. Comm.* **2009**, 1580-1582.

[6] Mandoj, F.; Nardis, S.; Pomarico, G.; Stefanelli, M.; Schiaffino, L.; Ercolani, G.; Prodi, L.; Genovese, D.; Zaccheroni, N.; Fronczek, F. R.; Smith, K. M. 6-Azahemiporphycene: a new member of the porphyrinoid family. *Inorg. Chem.* **2009**, *48*, 10346-10357.

[7] Stefanelli, M.; Mandoj, F.; Mastroianni, M.; Nardis, S.; Mohite, P.; Fronczek, F. R.; Smith, K. M.; Kadish, K. M.; Xiao, X.; Ou, Z.; Chen, P. Amination reaction on copper and germanium *β*-nitrocorrolates. *Inorg. Chem.* **2011**, *50*, 8281-8292.

[8] Singh, P.; Dutta, G.; Goldberg, I.; Mahammed, A.; Gross, Z. Expected and unexpected transformations of manganese(III) tris(4-nitrophenyl)corrole. *Inorg. Chem.* **2013**, *52*, 9349-9355.

[9] Paolesse, R.; Nardis, S.; Stefanelli, M.; Fronczek, F. R.; Vicente, M. G. H. Hemiporphycene from the Expansion of a Corrole Ring. *Angew. Chem. Int. Ed.* **2005**, *44*, 3047-3050.

[10] Fang, Y.; Mandoj, F.; Nardis, S.; Pomarico, G.; Stefanelli, M.; Cicero, D. O.; Lentini, S.; Vecchi, A.; Cui, Y.; Zeng, L.; Kadish, K.M. New example of hemiporphycene formation from the corrole ring expansion. *Inorg. Chem.* 2014, *53*, 7404-7415.

[11] Larsen, S.; McCormick, L. J.; Ghosh, A. Rapid one-pot synthesis of pyrrole-appended isocorroles. *Org. Biomol. Chem.* **2019**, *17*, 3159-3166.

[12] Ghosh, A. Electronic structure of corrole derivatives: insights from molecular structures, spectroscopy, electrochemistry, and quantum chemical calculations. *Chem. Rev.* **2017**, *117*, 3798-3881.

[13] Alemayehu, A. B.; Thomas, K. E.; Einrem, R. F.; Ghosh, A. The Story of 5d Metallocorroles: From Metal– Ligand Misfits to New Building Blocks for Cancer Phototherapeutics. *Acc. Chem. Res*. **2021**, *54*, 3095–3107.

[14] Nardis, S.; Mandoj, F.; Stefanelli, M. and Paolesse, R.;. Metal complexes of corrole. *Coordination Chemistry Reviews*, **2019**, *388*, 360-405.

[15] Alemayehu, A. B.; Vazquez-Lima, H.; Beavers, C. M.; Gagnon, K. J.; Bendix, J.; Ghosh, A. Platinum Corroles. *Chem. Comm*. **2014**, *50*, 11093-11096.

[16] Alemayehu, A. B.; McCormick, L. J.; Gagnon, K. J.; Borisov, S. M.; Ghosh, A. Stable Platinum(IV) Corroles: Synthesis, Molecular Structure, and Room-Temperature Near-IR Phosphorescence. *ACS Omega* **2018**, *3*, 9360-9368.

[17] Setsune, J. I.; Tsukajima, A.; Okazaki, N. Synthesis and structure of isocorrole metal complexes. *J. Porphyrins Phthalocyanines* **2009**, *13*, 256-265.

[18] Pomarico, G.; Xiao, X.; Nardis, S.; Paolesse, R.; Fronczek, F. R.; Smith, K. M.; Fang, Y.; Ou, Z.; Kadish, K. M.. Synthesis and characterization of free-base, copper, and nickel isocorroles. *Inorg. Chem.* **2010**, *49*, 5766-5774.

[19] Costa, R.; Geier III, G. R.; Ziegler, C. J.. Structure and spectroscopic characterization of free base and metal complexes of 5, 5-dimethyl-10, 15-bis (pentafluorophenyl) isocorrole. *Dalton Trans.* **2011**, *40*, 4384-4386.

[20] Foroutan-Nejad, C.; Larsen, S.; Conradie, J.; Ghosh, A. Isocorroles as Homoaromatic NIR-Absorbing Chromophores: A First Quantum Chemical Study. *Sci. Rep.* **2018**, *8*, 11952.

[21] Borisov, S. M.; Alemayehu, A.; Ghosh, A. Osmium-Nitrido Corroles as NIR Indicators for Oxygen Sensors and Triplet Sensitizers for Organic Upconversion and Singlet Oxygen Generation. *J. Mater. Chem. C* **2016**, *4*, 5822-5828.

[22] Lemon, C. M.; Powers, D.C.; Brothers, P.J.; Nocera, D. G. Gold corroles as near-IR phosphors for oxygen sensing. *Inorg. Chem.* **2017**, *56*, 10991-10997.

[23] Borisov, S. M.; Einrem, R. F.; Alemayehu, A. B.; Ghosh, A. Ambient-temperature near-IR phosphorescence and potential applications of rhenium-oxo corroles. *Photochem. Photobiol. Sci.* **2019**, *18*, 1166-1170.

[24] Einrem, R. F., Alemayehu, A. B., Borisov, S. M., Ghosh, A.; Gederaas, O. A. Amphiphilic Rhenium-Oxo Corroles as a New Class of Sensitizers for Photodynamic Therapy. *ACS Omega* **2020**, *5*, 10596-10601.

[25] Thomassen, I. K.; McCormick-McPherson, L. J.; Borisov, S. M.; Ghosh, A. Iridium Corroles Exhibit Weak Near-Infrared Phosphorescence but Efficiently Sensitize Singlet Oxygen Formation. *Sci. Rep.* **2020**, *10*, Art. No. 7551.

[26] Sahu, K.; Angeloni, S.; Conradie, J.; Villa, M.; Nayak, M.; Ghosh, A.; Ceroni, P.; Kar, S. NIR-emissive, singlet-oxygen-sensitizing gold tetra(thiocyano) corroles. *Dalton Trans.* **2022**, *51*, 13236-13245.

**TOC graphic**

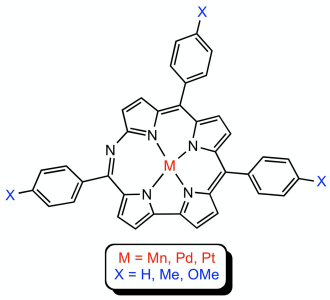


Synposis: Although transition metal 6-azahemiporphycenes are generally not luminescent, certain derivatives sensitize singlet oxygen formation; a Pd(II) derivative exhibits an impressive singlet oxygen quantum yield of 84%.